

1 *Technical note*

## 2 **First Evidence of Peat Domes in the Congo Basin** 3 **using LiDAR from a fixed-wing drone**

## 4 **Premières preuves de dômes de tourbe dans le bassin** 5 **du Congo utilisant un capteur LiDAR embarqué sur** 6 **un drone à voilure fixe**

7 **Ian J. Davenport<sup>1,\*</sup>, Iain McNicol<sup>1</sup>, Edward T. A. Mitchard<sup>1</sup>, Greta Dargie<sup>2,3</sup>, Ifo Suspense<sup>4</sup>,**  
8 **Brice Milongo<sup>4</sup>, Yannick E. Bocko<sup>5</sup>, Donna Hawthorne<sup>6</sup>, Ian Lawson<sup>7</sup>, Andy J. Baird<sup>2</sup>, Susan**  
9 **Page<sup>8</sup>, Simon L. Lewis<sup>2,3</sup>**

10 <sup>1</sup> School of GeoSciences, University of Edinburgh, Edinburgh EH9 3FF, UK; Ian.Davenport@ed.ac.uk,  
11 I.McNicol@ed.ac.uk, Edward.Mitchard@ed.ac.uk

12 <sup>2</sup> School of Geography, University of Leeds, Leeds LS2 9JT, UK; G.C.Dargie@leeds.ac.uk,  
13 A.J.Baird@leeds.ac.uk, S.L.Lewis@ucl.ac.uk

14 <sup>3</sup> Department of Geography, University College London, London WC1E 6BT, UK

15 <sup>4</sup> École Normale Supérieure, Université Marien Ngouabi, Brazzaville, Republic of the Congo;  
16 Ifo.Suspense@hotmail.fr, milongobrice@gmail.com

17 <sup>5</sup> Faculté des Sciences et Techniques, Université Marien NGOUABI, Brazzaville, Republic of the Congo;  
18 byannickenock@gmail.com

19 <sup>6</sup> School of Geography and Sustainable Development, University of St Andrews, Scotland, UK KY16 9AJ;  
20 dj43@st-andrews.ac.uk

21 <sup>7</sup> Department of Geography and Sustainable Development, University of St Andrews, St Andrews KY16  
22 9AL, UK; itl2@st-andrews.ac.uk

23 <sup>8</sup> School of Geography, Geology and the Environment, University of Leicester, Leicester LE1 7RH, UK;  
24 sep5@le.ac.uk

25 \* Correspondence: Ian.Davenport@ed.ac.uk

26 Received: 7 May 2020; Accepted: 6 July 2020; Published: 9 July 2020

27 **Abstract:** The world's most extensive tropical peatlands occur in the Cuvette Centrale depression in  
28 the Congo Basin, which store 30.6 petagrams of carbon (95% CI, 6.3–46.8). Improving our  
29 understanding of the genesis, development and functioning of these under-studied peatlands  
30 requires knowledge of their topography and, in particular, whether the peat surface is domed, as this  
31 implies a rain-fed system. Here we use a laser altimeter mounted on an unmanned airborne vehicle  
32 (UAV) to measure peat surface elevation along two transects at the edges of a peatland, in the  
33 northern Republic of Congo, to centimetre accuracy, and compare the results with an analysis of  
34 nearby satellite LiDAR data (ICESat and ICESat-2). The LiDAR elevations on both transects show an  
35 upward slope from the peatland edge, suggesting a surface elevation peak of around 1.8 m over ~20  
36 km. While modest, this domed shape is consistent with the peatland being rainfed. In-situ peat depth  
37 measurements and our LiDAR results indicates that this peatland likely formed at least 10,000 years  
38 BP in a large shallow basin ~40 km wide and ~3 m deep.

39 **Keywords:** peat; LiDAR; dome; carbon; ICESat; ICESat-2; swamp

40

41

42 **Résumé** : Les tourbières tropicales les plus étendues du monde se trouvent dans la dépression de la  
43 Cuvette Centrale dans le bassin du Congo, qui stocke 30,6 pétagrammes de carbone (IC à 95 %, 6,3 à  
44 46,8). Pour améliorer notre compréhension de la genèse, du développement et du fonctionnement de  
45 ces tourbières sous-étudiées, il faut connaître leur topographie, et en particulier déterminer si la  
46 surface de la tourbière est en forme de dôme, car ceci implique l'existence d'un système pluvial. Ici  
47 nous utilisons un altimètre laser embarqué sur un véhicule aérien sans pilote (UAV) pour mesurer  
48 l'élévation de la surface de la tourbe le long de deux transects aux bords d'une tourbière dans le nord  
49 de la République du Congo à la précision centimètre, et nous comparons les résultats aux analyses  
50 des données satellitaires d'un capteur LiDAR local (ICESat et ICESat-2). Les altitudes de LiDAR  
51 montrent sur tous les deux transects une pente ascendante à partir du bord de la tourbière, ce qui  
52 suggère un pic d'élévation de surface d'environ 1,8 m sur ~20 km. Bien que modeste, cette forme de  
53 dôme est compatible avec la tourbière qui est pluviale. Des mesures in situ de l'épaisseur de tourbe  
54 et nos résultats LiDAR indiquent que cette tourbière s'est probablement formée au moins 10 000 ans  
55 BP dans un bassin qui est grand mais peu profond, avec ~40km de large et ~3 m de profondeur.

56 **Mots clé** : tourbe ; LiDAR ; bombement, dôme ; carbone ; ICESat, ICESat-2 ; marais  
57

---

## 58 1. Introduction

59 Peatlands cover three percent of the Earth's land surface, but store a third of global soil carbon  
60 ([1,2]). The carbon in these systems is vulnerable to release due to land use and climate change,  
61 especially in the tropics where they are often drained and used for the cultivation of oil palm and  
62 pulpwood plantations. Indeed, it is estimated that 2.5 petagrams of carbon stored in peat swamps in  
63 SE Asia were released to the atmosphere over the period 1990 to 2015 through peat oxidation driven  
64 by a combination of peatland vegetation clearance and drainage [3,4]. However, such large carbon  
65 losses have not occurred so far in other tropical regions [5,6].

66 While it was once thought that only SE Asia has vast tracts of tropical peat, recent field  
67 measurements and analysis [5] have shown that the Cuvette Centrale depression in the central Congo  
68 Basin (Figure 1) also houses a large area of tropical peatland, recently estimated at 145,500 km<sup>2</sup> (95%  
69 CI 131,900-156,400 ) [5]. In terms of carbon, the Cuvette Centrale peatlands store 30.6 Pg C (95% CI  
70 6.3-46.8 Pg), suggesting that this region comprises a third of the tropical peatland carbon store [5].  
71 Dated peat cores suggest that the peatlands formed when central Africa became wetter at the end of  
72 the last glaciation, with in situ peat depth measurements along transects from peatland edges  
73 towards their centers showing an increase in peat depth, suggesting that large-scale shallow  
74 interfluvial basins gradually filled with peat during the Holocene [5].

75 These early hypotheses of the development of the central Congo peatlands need more data to  
76 refine them. In order to model and predict the response of peatlands to environmental changes, we  
77 need to understand how they function, which in part is related to their size and shape. Furthermore,  
78 when combined with peat depth measurements, the topography of the underlying mineral layer can  
79 be deduced, providing further information about the system. Peat domes or 'raised bogs' are found  
80 elsewhere in the tropics [5,7,8,9] typically indicating a rain-fed system, but investigations into the  
81 topography of the Cuvette Centrale using SRTM (Shuttle Radar Topography Mission) and ASTER  
82 (Advanced Spaceborne Thermal Emission and Reflection Radiometer) GDEM (Global Digital  
83 Elevation Model) did not reveal clear domes [5].

84 The attempt to map topography using SRTM and ASTER GDEM were limited in their precision  
85 and accuracy, and the failure to detect domes does not mean that domes do not exist: any elevation  
86 variation of ~3 m would be undetectable with these instruments [5]. The objective of the work  
87 reported herein was to quantify elevation variation across a large interfluvial peatland using (i) an  
88 unmanned aerial vehicle (UAV) fitted with LiDAR and (ii) satellite-based ranging LiDAR remote  
89 sensing instruments.  
90

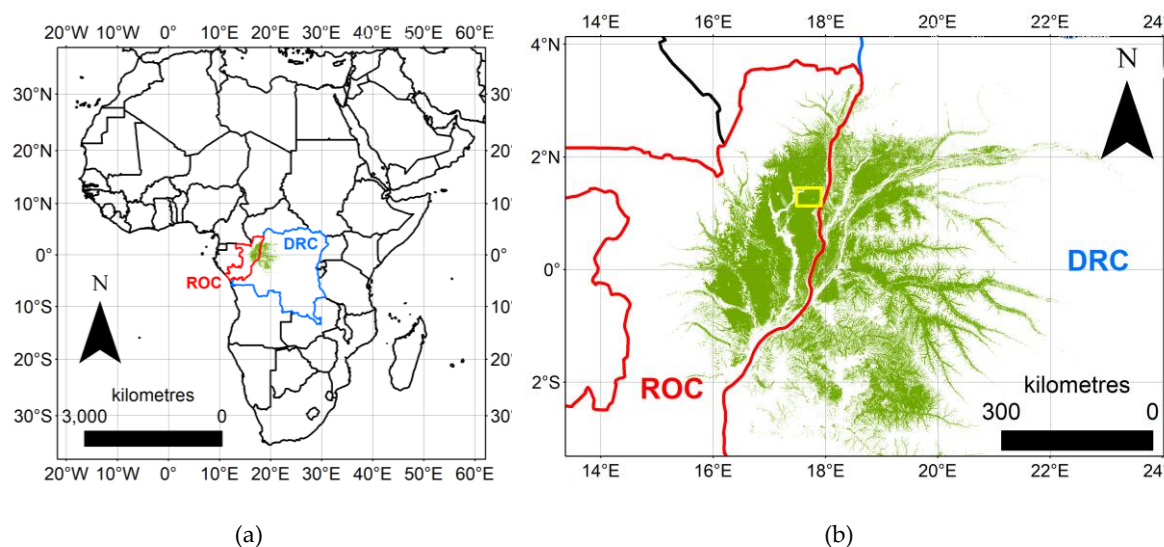


**Figure 1.** The location of the Centrale Cuvette peat deposit (green) in the Republic of Congo (ROC) and Democratic Republic of Congo (DRC) [5] (a) large scale; (b) local scale, field site in yellow

## 91 2. Materials and Methods

92 Figure 3 shows the forest area studied in this work. This region is covered by hardwood trees or  
 93 palm-dominated areas of swamp further from the peatland edge [2], between the Likouala-aux-  
 94 herbes and Ubangi rivers, and has water above or close to the surface year-round [5], containing  
 95 underlying peat as detailed below. The field site is in Likouala Department, Republic of Congo. Field  
 96 and remotely-sensed data were combined to build up a picture of peatland topography along a path  
 97 between Epena and Ekolongouma, as shown in Figure 3.

### 98 2.1 UAV LiDAR

99 A DelAir DT26x fixed-wing UAV equipped with a Riegl VUX-1UAV LiDAR scanner was  
 100 deployed from two sites, on the west and east of the peatland. From Ekolongouma, on the east,  
 101 (Figure 2) the UAV crossed the eastern edge of the forest at 17.901°E 1.204°N, flew at a 257° bearing  
 102 for 7.1 km and returned. The furthest 2.2 km of the flight line had been previously ground-surveyed  
 103 [5], and confirmed as peatland. On the west of the peatland, the UAV was launched from a site near  
 104 Epena, crossed the edge of the forest at 17.479°E 1.330°N and flew 7.9 km at a bearing of 124°, covering  
 105 a 5.8 km long profile from the western edge of the peatland before returning. The UAV operated at a  
 106 nominal altitude of 240 m above ground, and the LiDAR operated at an angle up to 30 degrees off-  
 107 nadir, creating in practice a swathe between 330 m and 350 m wide. Laser beam divergence was 0.5  
 108 mrad, generating a spot diameter at ground level of about 12 cm. Data was recorded on the outgoing  
 109 and return legs of each flight, with trajectories differing only by a few meters. A differential GPS  
 110 station was operated near the launch sites for a 24 hour period to establish an accurate position, and  
 111 during each mission, to allow georeferencing of the LiDAR return elevations to centimetric accuracy.  
 112 The regions over which data were gathered are shown in Figure 3.

113 While this is a labour-intensive approach, requiring months of planning and weeks of effort to  
 114 cover an area of a few square kilometres, accurate GNSS measurements of the peat surface are  
 115 infeasible at this site because of the dense tree canopy, meaning there is no sufficiently-accurate field  
 116 alternative. The 12-cm spot diameter and point density up to 35 m<sup>-2</sup> provided by UAV LiDAR should  
 117 allow ground measurements in most forests, and we are actively testing the system in Peru and  
 118 Gabon. The main requirements are a clear site for launch and landing, and a line-of-sight from the  
 119 antenna to the UAV, which is a function of the site geometry, and can be calculated from antenna  
 120 height, canopy height, distance from antenna to forest edge, and flight altitude.

121



122  
123  
124 **Figure 2.** The UAV prepared for launch site at the cleared site near Ekolongouma, and peat depth field  
125 measurements being made in the hardwood forest.  
126

127 To estimate the ground topography along each acquisition, a straightened trajectory line was  
128 drawn between the entry point of the UAV to the peat area and the point where it turned for the  
129 return trip. Ground elevation for each 1 m segment of the line was estimated by finding the return  
130 with the lowest elevation amongst the returns between the segment and the edges of the swathe. This  
131 introduces an overall downward bias, as these points will have the largest downward error. The  
132 points acquired during the outward and return flights were processed separately, producing a pair  
133 of ground-level estimates for each 1 m segment. The mean difference and root mean square difference  
134 (RMSD) between these pairs was calculated to evaluate the measurements. The canopy top elevation  
135 was estimated from the local maximum return over 100 m.  
136

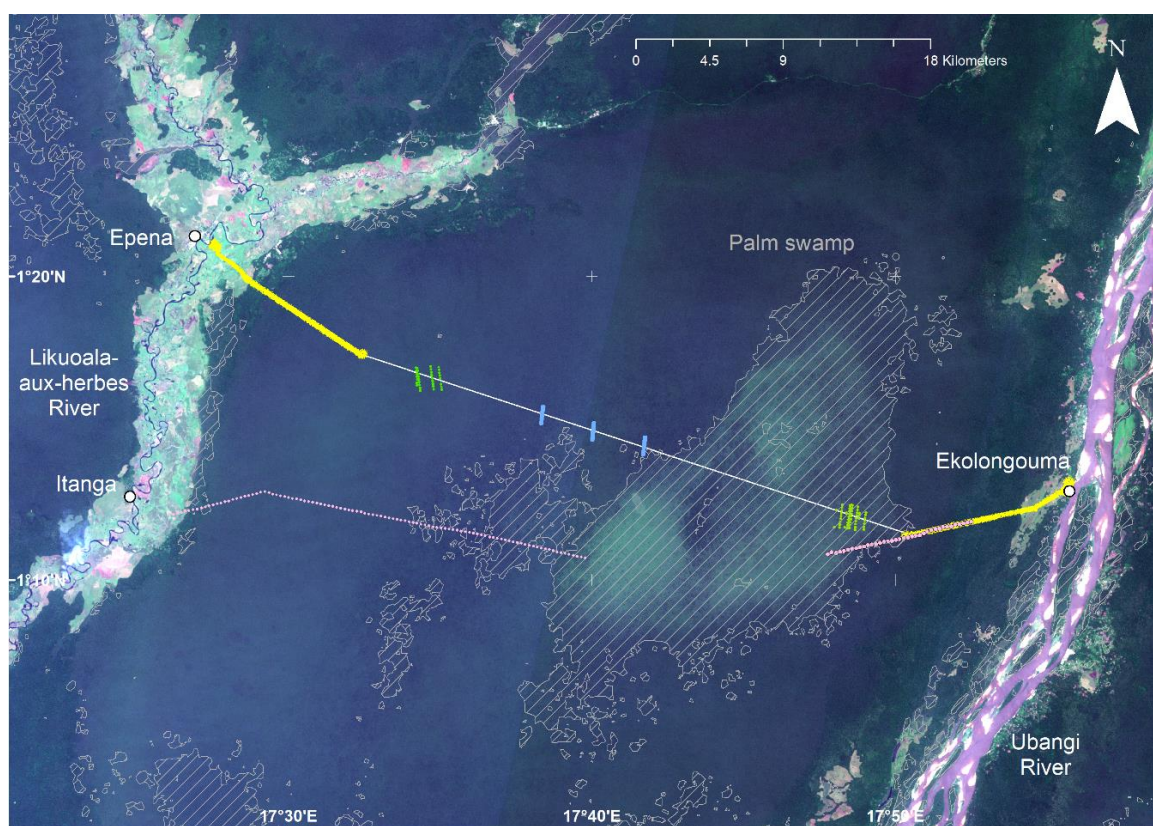


**Figure 3.** The locations of acquired data **UAV LiDAR**, **ICESat**, **ICESat-2**, **field-measured peat depth** and the area believed to be palm swamp (white hatched) [5]. A white line joins the LiDAR transects forming a path between the peat edges 43.8km long, compared to 43.3km direct-line distance. Background image is a Sentinel-2 composite, Copyright European Space Agency.

## 137 2.2 Peat Depth Field measurements

138 Peat depth (where peat is defined as material consisting of at least 65% organic matter to a depth  
 139 of at least 0.3 m) was estimated every 250 m along transects established during three field expeditions  
 140 [5], starting on each side where savannah gives way to hardwood forest, using a pole pushed through  
 141 the peat until it reached the subsurface clay. More precise measurements were made every km along  
 142 the two edge transects, and every 4 km along the central transect using loss on ignition in a laboratory  
 143 to assess the organic matter content. The pole measurements were calibrated to the laboratory  
 144 methods using 44 peat depth estimates derived from both the pole and laboratory methods [5]. One  
 145 transect started from the Ubangi River side 3 km in from the forest edge at Ekolongouma village  
 146 (17.87514°E, 1.19859°N) and proceeded on a 257° bearing for 9 km, finding peat from 4.5 km into the  
 147 forest onwards. A second transect started from the Likouala-aux-herbes River and reached 6 km on  
 148 a 78° bearing from Itanga village (17.43449°E, 1.20250°N), finding peat consistently from about 1.25  
 149 km into the forest. A third continued this transect at a bearing of 102° in the direction of the  
 150 Ekolongouma transect, also finding peat consistently from the beginning of the transect for 20 km.

151 To determine the topography of the subsurface on which the peat is developing, we need  
 152 measurements of ground elevation and peat depth at the same location. While the flight line in the  
 153 east coincides with the eastern field peat measurement transect, and so can be compared directly to  
 154 LiDAR elevation estimates, the western transect from Itanga starts some 12 km south of the aerial  
 155 flight line, and approaches it at the centre of the peat (Figure 3). To compare the western field data  
 156 with the aerial data, we need to estimate where the peat begins beneath the flight line. We used  
 157 normalised difference vegetation index (NDVI) profiles along the field transect and flight-line  
 158 derived from Sentinel-2 bands four and eight. Along the field transect from Itanga, the mean NDVI,  
 159 averaged over 500 m, dropped nearly monotonically from 0.602 at the edge of the forest to 0.557 at a

160 distance of 2.5 km into the forest. It dropped below 0.59 at the start of the continuous peat  
161 measurements, 1 km into the forest at longitude 17.452°E. Along the flight-line from Epena, NDVI  
162 dropped similarly, passing 0.59 at 17.493°E, about 1.3 km into the forest. We approximate, therefore,  
163 that the peat cover along the Epena line starts around 17.493°E. For a rough comparison between the  
164 datasets, the measurement corresponding to the western end of the peat transect is plotted at  
165 17.493°E, the final point in the centre of the field remains unmoved, and all points between are  
166 proportionately shifted.

### 167 2.3 ICESat and ICESat-2

168 The Geoscience Laser Altimeter System (GLAS) instrument on the ICESat platform used a  
169 1064 nm laser with a footprint about 65 m in diameter between 2003 and 2010, and light returns were  
170 processed to estimate surface from the first significant return (the Level 1B product GLAH06 [10])  
171 and terrain from the last return (the level 2 product GLAH14 [11,12]) elevations. The Advanced  
172 Topographic Laser Altimeter System (ATLAS) instrument on the ICESat-2 platform was launched in  
173 September 2018, and pulses a 552 nm laser at the Earth's surface, illuminating a 17 m-diameter  
174 footprint. The ATL03 product [13], comprising latitude, longitude and elevation for each received  
175 photon, was used in this work.

176 No ICESat or ICESat-2 tracks crossed either of the UAV LiDAR transects; however both  
177 instruments provided returns in the gap between the transects, and the returns around the line  
178 between the transects, drawn in white in Figure 3, were extracted. Two ICESat tracks crossed the line  
179 between the two transects, and the GLAH06 and GLAH14 elevation estimates were analysed. One  
180 ICESat-2 track crossed the line, and the ATL03 returns in the region around this line were analysed.  
181 Since these products had not previously been tested for ground/vegetation discrimination in these  
182 areas, the GLAH06, GLAH14 and ATL03 data were analysed by building local histograms of  
183 elevations, to try to identify the ground elevation in the context of the return distribution, and by  
184 comparison with the other data sources.

### 185 2.4 TanDEM-X

186 The Tandem-X 90 digital elevation model [14] is a 90m DSM derived from the TanDEM-X X-  
187 band synthetic aperture radar (SAR) instrument via interferometry. The elevations corresponding to  
188 the path illustrated in Figure 3 were extracted from this dataset.

## 189 3. Results and Discussion

### 190 3.1 UAV LiDAR

191 The minimum returns per 1 m along each transect for the outgoing and return transects starting  
192 from the two locations on the edge of the peatland, are shown in Figure 4. The return flight to  
193 Ekolongouma suffered a data loss, and 400 m of the returns in the peat area could not be processed  
194 and analysed. For the Epena flight, the extent of peat was inferred as above, and the plot shows  
195 estimated elevation over that extent.

196 For the Ekolongouma flight, the mean difference between the outgoing and return flights' lowest  
197 points for each 1 m segment was 0.0064 m, with an RMSD between the outgoing/return pairs of  
198 0.13 m. For the Epena flight, the mean difference between outward and return ground estimates was  
199 0.021 m, with an RMSD of 0.29 m. The Epena measurements likely have a larger uncertainty because  
200 of the longer mission length. The Ekolongouma measurements used in the analysis were taken over  
201 4 km of flying during about 6 minutes, whereas the Epena measurements cover a total of 12 km with  
202 a flight time of about 17 minutes, allowing more time for GNSS elevation drift to affect measured  
203 heights. The low mean differences indicate a local consistency in elevation measurement over the  
204 duration of the flights of 2 cm, suggesting that the GNSS location of the aircraft and laser timing  
205 measurement contribute only a small systematic uncertainty. The RMSD is due to a combination of  
206 the individual laser return timing uncertainty and ground level vegetation variability. For both sites,

207 fitting a linear trend shows a slope upwards away from the edge of the peatland of around 0.00012  
 208 m.m<sup>-1</sup> for the eastern Ekolongouma side, and around 0.00015 m.m<sup>-1</sup> on the western Epena side.

209 Since this analysis uses the lowest of around 5000 measurements corresponding to each 1 m  
 210 stretch, the uncertainty in each measurement will give rise to a systematic downward bias in the  
 211 ground level estimate. The scatter in Figure 4, and similar work [15] suggests this will be about 20  
 212 cm.  
 213

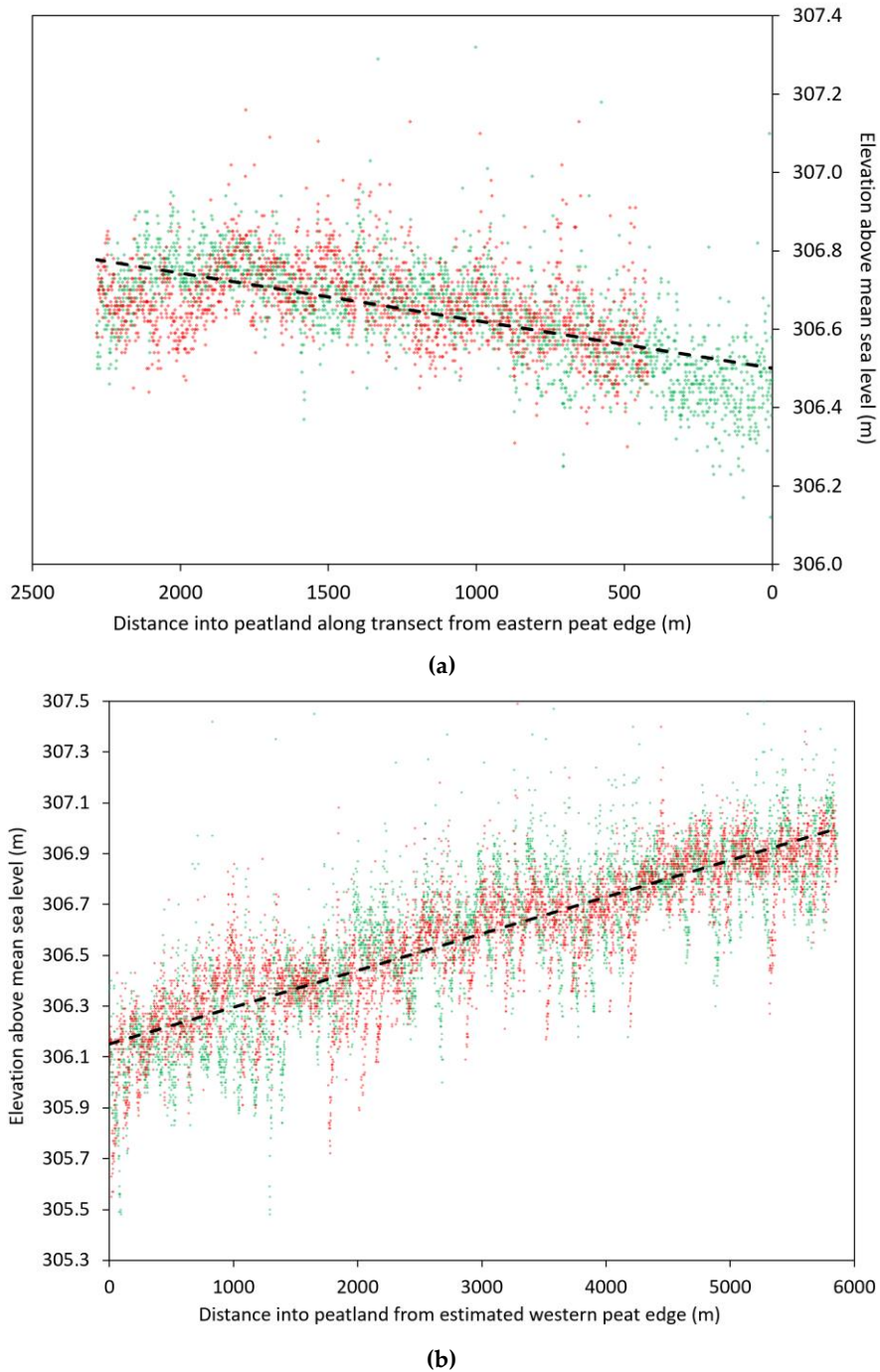


**Figure 4.** Estimated ground elevation points per meter along UAV transect from the estimated peat edge. Green points are derived from the outgoing flight, red returning. (a). Ekolongouma. The total transect is 2269 m long, for 1862 m of which we have both outgoing and returning flight data. The fitted line slope is 0.121 m.km<sup>-1</sup>. (b). Epena. Total transect length is 5861 m. The fitted line slope is 0.145 m.km<sup>-1</sup>.

### 214 3.2 ICESat GLAH14 (terrain) and GLAH06 (surface)

215 ICESat tracks crossed the line joining the two UAV transects several times between 25th  
 216 February 2003 and 23rd March 2005. In the west, track 402 crossed at 17.579°E 1.278°N and in the east  
 217 track 156 crossed at 17.809°E 1.201°N. The GLAH06 and GLAH14 returns not classified as noise  
 218 within 0.015° latitude of these two locations were analysed. As there were only between 19 and 61  
 219 points in each of these data sets, and the tracks are closely grouped, each area and return type was  
 220 treated as one group.  
 221

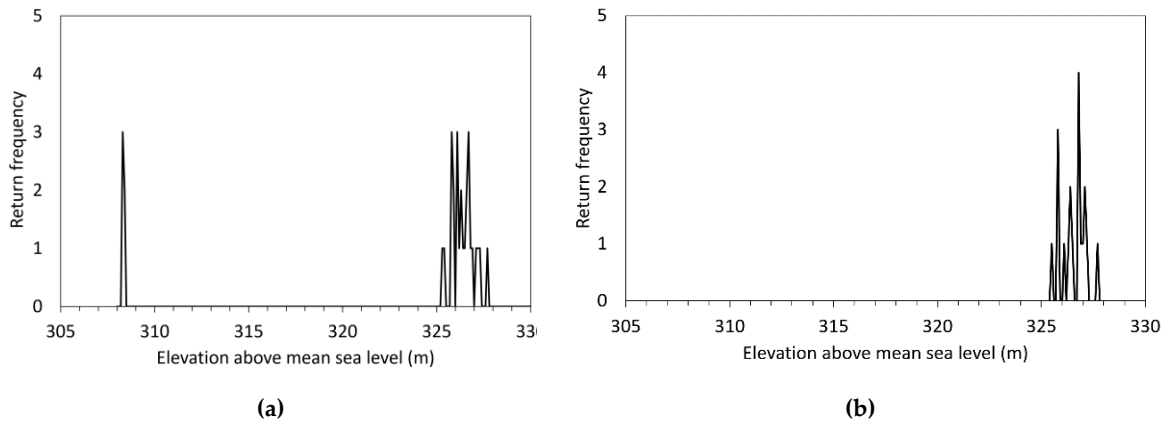


**Figure 5.** ICESat GLAS west region returns, (a) GLAH06 (b) GLAH14.

222  
 223 In the west (Figure 5 (a)), the 33 GLAH06 returns showed a bimodal distribution, with five  
 224 elevation estimates between 308.27 m and 308.37 m and a mean of 308.30 m, potentially representing  
 225 the ground, and a cluster of 28 between 325.24 m and 327.65 m with a mean of 326.34 seeming to  
 226 represent the canopy as mapped by TanDEM-X. There were also two outliers, at 653.52 m and 663.05  
 227 m. The 19 GLAH14 returns (Figure 5 (b)) showed points with a unimodal distribution between 325.44  
 228 m and 327.61 m with a mean of 326.52 m, close to the local TanDEM-X elevations, strongly suggesting  
 229 that the GLAH14 data in this case corresponds to the canopy rather than the underlying terrain.

230 In the east track, the 61 GLAH14 (terrain) returns (Figure 6 (a)) showed a unimodal distribution,  
 231 around 317 m above mean sea level, and the 31 GLAH06 returns showed a unimodal distribution  
 232 (Figure 6 (b)) centred at 316 m. Since the terrain-canopy separation should be 10 m or more, both of  
 233 these seem to be representing either canopy or terrain. The nearest UAV measurements show the  
 234 terrain about 10 m below this, and TanDEM-X shows an elevation of 316–318 m in this region. The  
 235 classification, as shown in Figure 3, indicates that this area is palm-dominated, whereas the other  
 236 satellite and UAV altimetry used here was acquired over hardwood tree regions, suggesting that the  
 237 larger leaves of the palm swamp forming a more even and lower canopy are preventing ground  
 238 returns.

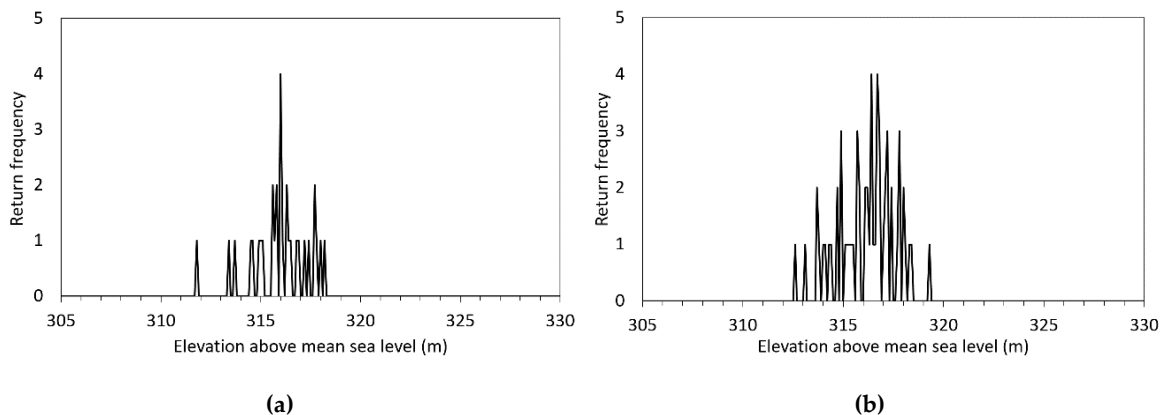


**Figure 6.** ICESat GLAS east region returns (a) GLAH06, (b) GLAH14.

## 239 3.3 ICESat-2 ATLO3

240 ICESat-2 ATLAS photon returns crossing the line between the UAV transects were only available  
 241 for track 236 on 13th April 2019. ICESat-2 beams are divided into strong and weak pairs to enhance  
 242 radiometric dynamic range [16]. The strong/weak spot pair tracks crossed this line at three points:  
 243 17.639°E 1.258°N, 17.667°E, 1.248°N and 17.695°E, 1.240°N. Photon return locations from within a  
 244 0.005 degree N-S extent of these points were extracted, noise-classified points removed, and  
 245 histograms formed of the remaining points, numbering around 250 photon returns for each weak  
 246 spot and 1000 returns for each strong spot. Given the large number of returns per spot and the  
 247 relatively high separation, the returns for each spot were analysed separately. All six spot sets  
 248 returned histograms (Figure 7) showing distributions consistent with a discrete ground return and  
 249 an extended vegetation return. The returns apparently corresponding to a ground return were  
 250 estimated by identifying the ground return spike with the estimated 1.6 m elevation instrument  
 251 uncertainty scatter [17], and a mean used to estimate the ground elevation for each spot. The mean  
 252 estimated ground elevation over the six spots is 309.18 m, and the mean location is at 17.67E 1.25N,  
 253 within 0.01E of the W-E centre of the path through the peatland.  
 254

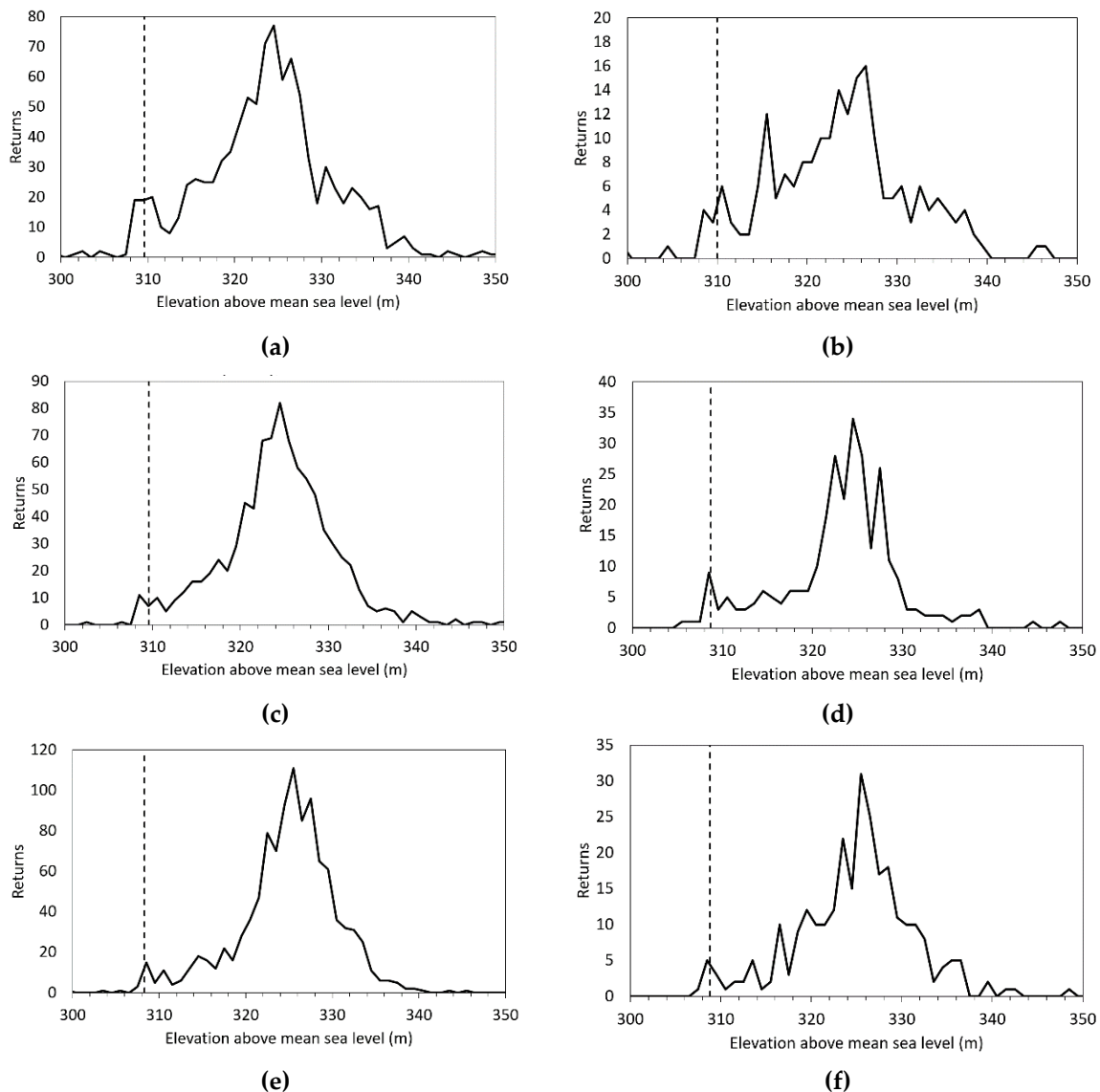
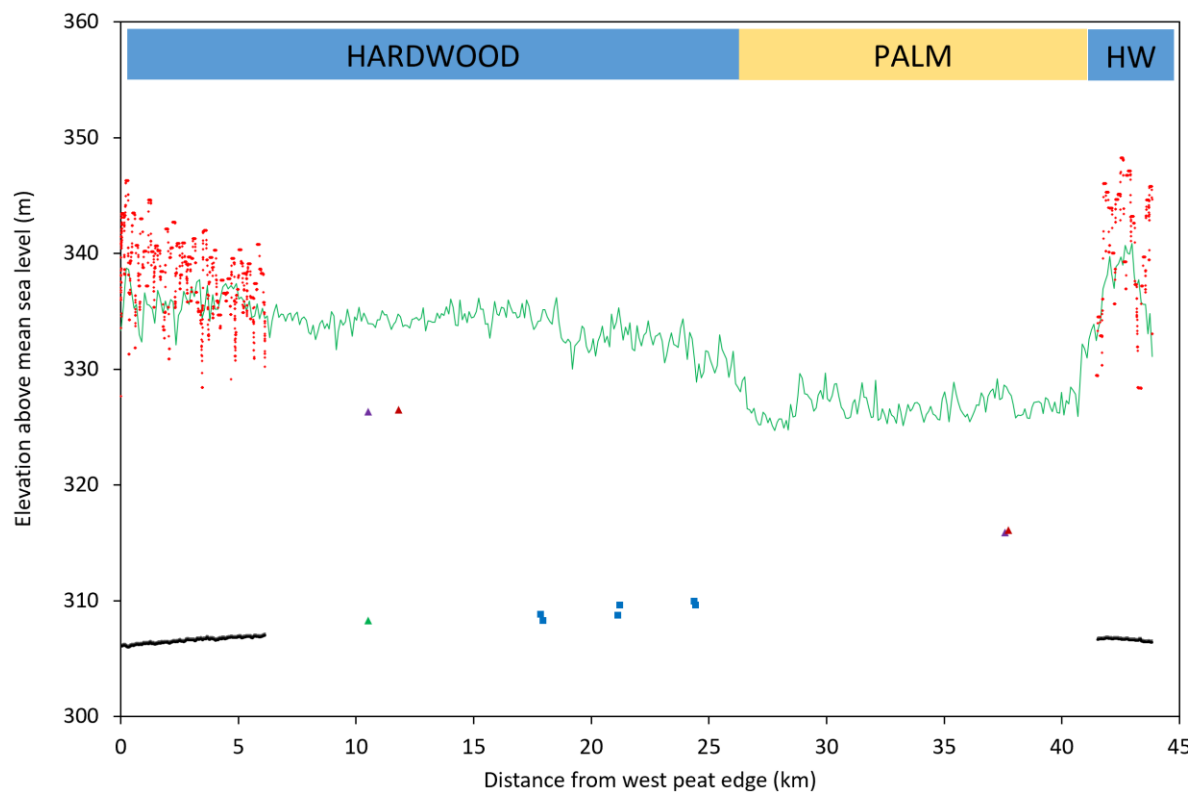


**Figure 7.** ICESat-2 ATLAS return histograms for each spot, inferred ground elevation indicated by a dashed line. (a) GT1L (strong), (b) GT1R (weak), (c) GT2L (strong), (d) GT2R (weak), (e) GT3L (strong), (f) GT3R (weak). Abscissa scales varied for legibility.

## 255 3.4 TanDEM-X

256 Figure 8 shows the elevations along the Figure 3 path between the peat edges, derived as above,  
 257 and the TanDEM-X profile along the same path.



258

259 **Figure 8.** Measured elevations along the Figure 2 Epena-Ekolongouma path from ICESat GLAH06  
 260 (▲ ground, ▲ canopy), GLAH14 (▲), ICESat-2 ground returns (■), UAV LiDAR canopy (•), UAV LiDAR  
 261 ground 100-m moving average (—), TanDEM-X (—). Forest type at top of figure.

262

263 Figure 9 shows all of the acquired data believed to describe the ground elevation along the west-  
 264 east path from Epena to Ekolongouma shown in Figure 3. Because of the estimated downward bias  
 265 of the UAV LiDAR ground elevation estimates, a 20 cm upward error bar has been marked. Error  
 266 bars for ICESat have been marked as 2.0m [18], ICESat-2 as 1.6m [17]. While the sparsity of data  
 267 around the centre of the peatland precludes identifying the precise shape, a parabola has been fitted  
 268 to the data with a peak of 308.2 m above mean sea level, 306.1 m at the western edge of the peat and  
 269 306.7 m at its eastern edge, suggesting a peat dome with a highest point approximately 1.8 m above  
 270 its edges. While this line falls 1-2 m below the satellite-based measurements, we are much more  
 271 confident in the UAV-based measurements and, given the slopes at either edge, a slope increase to  
 272 reach the ICESat-2 central elevations indicated seems implausible, and we have to conclude that the  
 273 ICESat and ICESat-2 measurements exhibit a systematic upward bias.

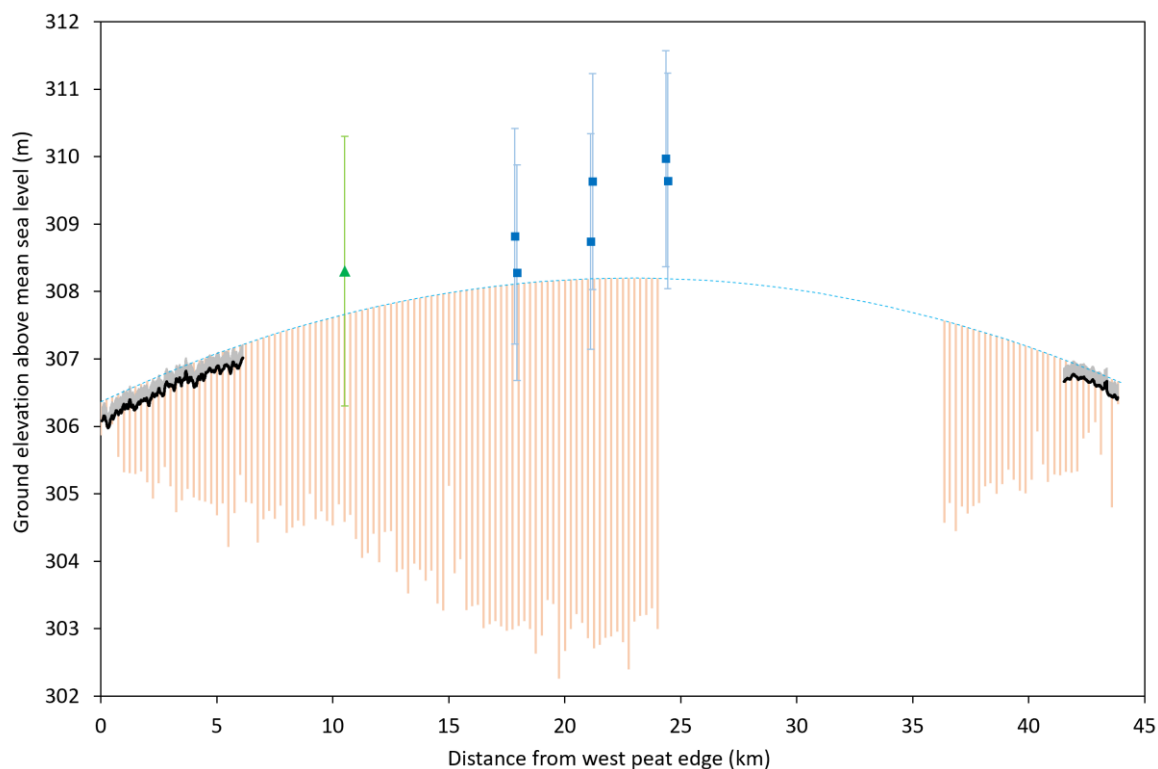
274

275 Vertical lines below the fit indicate the depth of the peat, approximated in the west as discussed  
 276 above, showing that the peat depth is around twice the elevation increase, and it is reasonable to infer  
 277 that the peatland originated in a shallow basin at 3-4 m in depth, though if the peat peak is higher  
 278 than estimated, the basin depth would be correspondingly shallower.

278

279 Due to the limited range of the UAV, a complete transect of high-quality LiDAR data across the  
 280 entire peatland was not possible. While we have focused on the simplest, most likely interpretation  
 281 of the data, we cannot exclude the possibility of other, more complex topographies (Figure 10). The  
 282 shape and size of a peatland, including the formation of a peat dome, result from complex feedbacks  
 283 between climate, litter production, peat decay, peat permeability (hydraulic conductivity) and water-  
 284 balance processes, including surface and subsurface water flows on and through the peat (e.g.  
 [19],[20],[21],[22]). Currently, we know little about the controls on peat formation at the site and it is

285 important to recognise that other topographies are consistent with our data as shown in Figure 10.  
 286 Future work on the topography of Congolese peatlands could usefully focus on (i) validating the  
 287 UAV LiDAR measurements to reduce uncertainty in the peak height by deploying on a platform with  
 288 a longer range, and (ii) analysing newly-available data from the GEDI LiDAR instrument on the  
 289 International Space Station [23]. We are investigating options for an alternative aircraft platform, and  
 290 have analysed the initial 8-week GEDI data release, which included some acquisitions along our  
 291 transect which were unfortunately blocked by cloud cover.  
 292

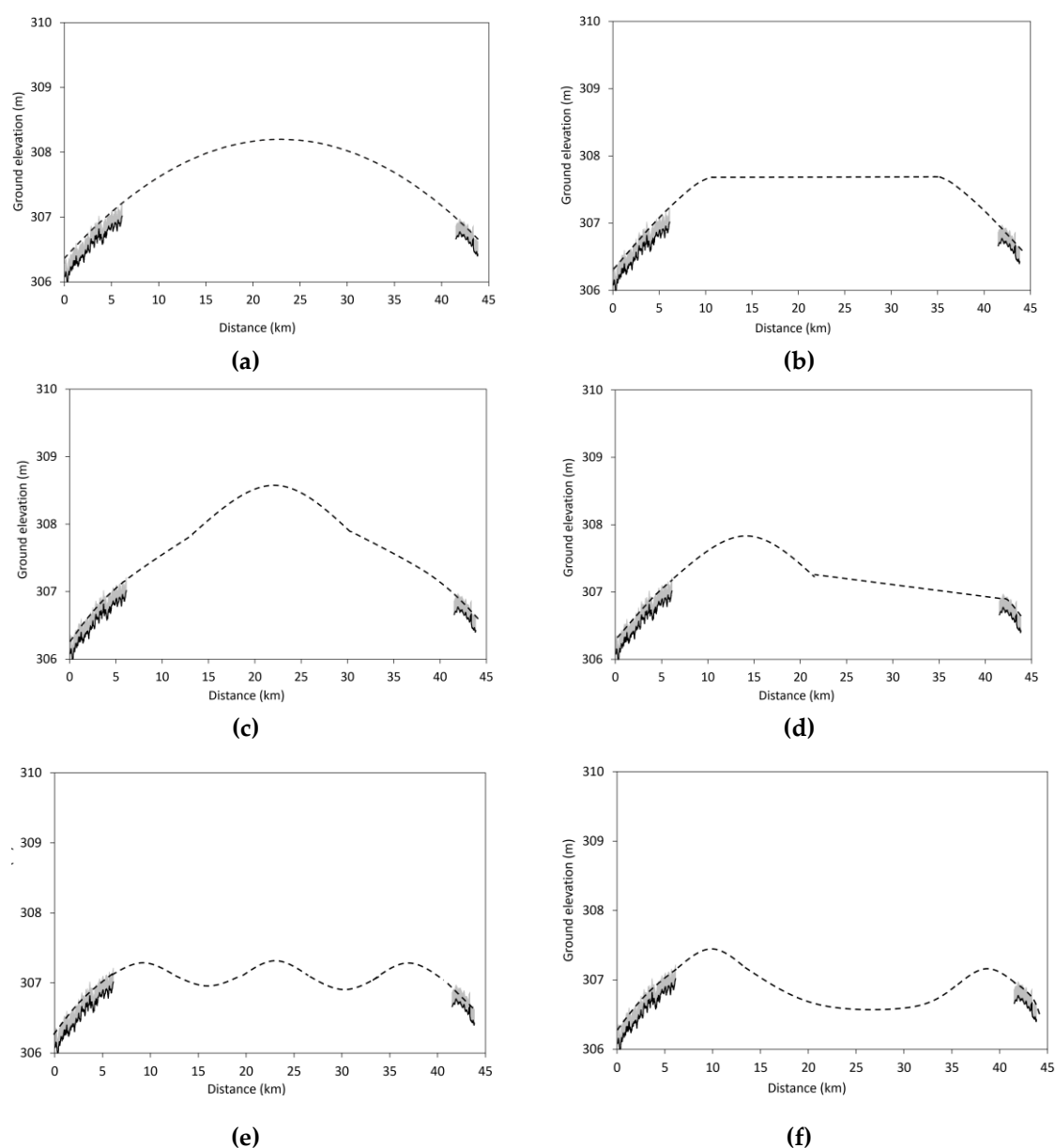


293 **Figure 9.** Plot of peat depths (orange vertical bars), ground elevations from ICESat ( $\blacktriangle$ ), ICESat-2 ( $\blacksquare$ ), UAV  
 294 LiDAR 100m moving average (black line with grey error bars) and parabolic fit (blue dashed line) with a peak  
 295 at 308.2m, along the Figure 3 Epena-Ekolongouma path.

#### 296 4. Conclusions

297 Two transects of UAV LiDAR data have defined the edges of a large peatland in the central  
 298 Congo basin. The data shows a gentle slope from the edges, towards the centre of the peatland,  
 299 suggesting, albeit not proving, that the surface is domed. This is the first evidence of a domed  
 300 peatland surface surveyed in this region. This peatland has a span of 45 km east-west, and reaches a  
 301 dome height of 1.8 m, as estimated from a parabolic fit to the LiDAR data, and a larger dome height  
 302 of 3.0 m from simple extrapolation of the mean slope of both LiDAR transects from edge to centre of  
 303 the peatland. Peat depth measurements indicate that the underlying topography is a shallow basin;  
 304 the peat reaches a maximum depth of 5.9 m at 17.4 km from the western peatland edge. By contrast  
 305 peat domes in south-east Asia with diameters greater than 40 km have a steeper topography with  
 306 domes rising up to 20 m (e.g. [24]). Smaller peatlands in south-east Asia (diameters of  $\sim 10$  km) also  
 307 have steeper topography, rising to six or more metres above their margins (e.g. [25,26]). SE Asian  
 308 peatlands also have greater peat depths and can be between 10 and 20 m deep towards their centres  
 309 (e.g. [24]). In Amazonian Peru, only small domes 10 km in diameter and  $< 2$  m in height, with 3–7 m  
 310 of peat, have so far been reported ([7,27]). It therefore appears that the Congolese example is unusual  
 311 in being both large and shallow. This may relate to the relatively low rainfall in central Congo ( $\sim 1,700$   
 312 mm yr $^{-1}$ ) compared to SE Asian and Peruvian sites ( $\sim 3,000$  mm yr $^{-1}$ ) resulting in lower peat  
 313 accumulation rates in the central Congo compared to the other sites (table 1 in ref [5]).

314



315 **Figure 10.** Potential peat dome morphologies: a) Convex dome, b) Plateau dome, c) Stepped dome, d)  
 316 Sloping dome, e) Undulating dome, f) Double dome with intervening basin.

317 **Author Contributions:** S.L.L., E.T.A.M. and G.D. conceived the experiment; I.M., I.J.D., G.D., S.L.L., I.S., Y.B.,  
 318 B.M. organised and conducted the fieldwork; I.J.D. analysed and interpreted the measurements and wrote most  
 319 of the manuscript; D.H., A.B., and I.L. evaluated the implications; S.P., I.L., A.B., S.L.L. reviewed and edited the  
 320 manuscript.

321 **Funding:** This work was funded by CongoPeat, a NERC Large Grant (NE/R016860/1) to S.L.L. and E.T.A.M.  
 322 (UAV data collection, I.J.D. time), a NERC Open CASE Studentship to S.L.L., I.L. and G.D. and a Phillip  
 323 Leverhulme Prize to S.L.L. (peat depths).

324 **Acknowledgments:** We are grateful for the cooperation of the villages of Ekolongouma and Epena, the  
 325 government of the Republic of Congo, the Likouala Prefecture, the Ministry of Environment and Tourism,  
 326 Marien N'gouabi University and the World Conservation Society (WCS) Congo for assistance. Mbongo Roger  
 327 of the WCS, Abia Platini, Angoni Tresor, Bobetolo Jean Bosco, Mouapeta Fulgence, Elongo Bienvenu, Fatty  
 328 Carlos, Mokondo Ismael, Iwango Michel, Mobembe Amalphi, Moniobo Belen Ekous, Ngongo Guy and Chancel  
 329 helped collect the field data.

330 **Conflicts of Interest:** The funders had no role in the design of the study; in the collection, analyses, or  
331 interpretation of data; in the writing of the manuscript, or in the decision to publish the results.

332

## 333 References

- 334 1. Rydin, H.; Jeglum, J. K. *The Biology of Peatlands*, Oxford Univ. Press, 2006, pp. 230–233.
- 335 2. Page, S. E.; Rieley, J. O. & Banks, C. J. Global and regional importance of the tropical peatland carbon pool.  
336 *Glob. Change Biol.* 2011, 17, 798–818.
- 337 3. Mitchard, E.T.A. The tropical forest carbon cycle and climate change, *Nature*, **2018**, 559, 527–534
- 338 4. Miettinen, J.; Hooijer, A.; Vernimmen, R.; Liew, S.C.; Page, S.E. From carbon sink to carbon source:  
339 extensive peat oxidation in insular Southeast Asia since 1990. *2017 Environmental Research Letters*, 12  
340 024014 (<http://iopscience.iop.org/1748-9326/12/2/024014>)
- 341 5. Dargie, G.C.; Lewis, S.L.; Lawson, I.T.; Mitchard, E.T.A.; Page, S.E.; Bocko, Y.E.; Ifo, S.A. Age, extent and  
342 carbon storage of the central Congo Basin peatland complex. *Nature*, **2017**, 542 (7639). pp. 86–90. ISSN 0028-  
343 0836 <https://doi.org/10.1038/nature21048>
- 344 6. Lähteenoja, O. & Page, S. High diversity of tropical peatland ecosystem types in the Pastaza-Marañón  
345 basin, Peruvian Amazonia. *J. Geophys. Res. Biogeosci.* 116, G02025 (2011).
- 346 7. Anderson, J. A. R., 1983, Tropical peat swamps of western Malesia, in Gore, A. J. P., ed., *Ecosystems of the*  
347 *world*, v. 4B: Amsterdam, Elsevier, p. 181–1
- 348 8. Lähteenoja, O.; Ruokolainen, K.; Schulman, L.; Alvarez, J. "Amazonian floodplains harbour minerotrophic  
349 and ombrotrophic peatlands." *Catena* 79, no. 2 (2009): 140–145.
- 350 9. Phillips, S.; Rouse, G.E.; Bustin, R.M. "Vegetation zones and diagnostic pollen profiles of a coastal peat  
351 swamp, Bocas del Toro, Panama." *Palaeogeography, Palaeoclimatology, Palaeoecology* 128, no. 1–4 (1997):  
352 301–338.
- 353 10. Zwally, H. J.; Schutz, R.; Bentley, C.; Bufton, J.; Herring, T.; Minster, J.; Spinhirne, J.;  
354 Thomas, R. 2014. *GLAS/ICESat L1B Global Elevation Data, Version 34*. [GLAH06]. Boulder, Colorado USA.  
355 NASA National Snow and Ice Data Center Distributed Active Archive Center.  
356 doi: <https://doi.org/10.5067/ICESAT/GLAS/DATA126>. Accessed 01/Aug/2019.
- 357 11. Zwally, H. J.; Schutz, R.; Bentley, C.; Bufton, J.; Herring, T.; Minster, J.; Spinhirne, J.;  
358 Thomas, R. 2014. *GLAS/ICESat L2 Global Land Surface Altimetry Data, Version 34*. [GLAH14]. Boulder,  
359 Colorado USA. NASA National Snow and Ice Data Center Distributed Active Archive Center.  
360 doi: <https://doi.org/10.5067/ICESAT/GLAS/DATA227>. Accessed 01/Aug/2019.
- 361 12. Ballhorn, U.; Jubanski, J.; Siegert, F. ICESat/GLAS Data as a Measurement Tool for Peatland Topography  
362 and Peat Swamp Forest Biomass in Kalimantan, Indonesia *Remote Sens.* 2011, 3, 1957–1982;  
363 doi:10.3390/rs3091957
- 364 13. Neumann, T. A.; Brenner, A.; Hancock, D.; Robbins, J.; Luthcke, S. B.; Harbeck, K.; Lee, J.; Gibbons, A.;  
365 Saba, J.; Brunt, K. 2019. *ATLAS/ICESat-2 L2A Global Geolocated Photon Data, Version 1*. ATL03. Boulder,  
366 Colorado USA. NSIDC: National Snow and Ice Data Center.  
367 doi: <https://doi.org/10.5067/ATLAS/ATL03.001>. Accessed 13/Aug/2019.
- 368 14. Hawker, L., Neal, J., Bates, P., 2019. Accuracy assessment of the TanDEM-X 90 digital elevation model for  
369 selected floodplain sites. *Remote Sens. Environ.* 232, 111319. <https://doi.org/10.1016/j.rse.2019.111319>.
- 370 15. Bakula, K.; Ostrowski, W.; Pilarska, M.; Szender, M.; Kurczynski, Z. Evaluation and calibration of fixed-  
371 wing uav mobile mapping system equipped with lidar and optical sensors. *Int. Arch. Photogramm. Remote*  
372 *Sens. Spatial Inf. Sci.* 2018, XLII-1, 25–32.
- 373 16. Neumann, T. A., Martino, A. J., Markus, T., Bae, S., Bock, M. R., Brenner, A. C., et al. (2019). The Ice, Cloud,  
374 and Land Elevation Satellite–2 mission: A global geolocated photon product derived from the Advanced  
375 Topographic Laser Altimeter System. *Rem. Sen. Environ.*, 233, 111325.  
376 <https://doi.org/10.1016/j.rse.2019.111325>.
- 377 17. C. Wang, X. Zhu, S. Nie, X. Xi, D. Li, W. Zheng, and S. Chen, "Ground elevation accuracy verification of  
378 ICESat-2 data: a case study in Alaska, USA," *Opt. Express* 27, 38168–38179 (2019).  
379 <https://doi.org/10.1364/OE.27.038168>
- 380 18. Ensle, F., Heinzl, J., Koch, B., 2014. Accuracy of vegetation height and terrain elevation derived from  
381 ICESat/GLAS in forested areas. *Int. J. Appl. Earth Obs. Geoinf.* 31, 37–44.
- 382 19. Belyea, L.R., and Baird, A.J. 2006. Beyond "the limits to peat bog growth": Cross-scale feedback in peatland  
383 development. *Ecological Monographs* 76, 299–322.

- 384 20. Morris, P.J., Baird, A.J., and Belyea, L.R. 2012. The DigiBog peatland development model: Ecohydrological  
385 simulations in 2D. *Ecohydrology* 5, 256–268.
- 386 21. Froking, S., Roulet, N.T., Tuittila, E., Bubier, J.L., Quillet, A., Talbot, J., and Richard, P.J.H. 2010. A new  
387 model of Holocene peatland net primary production, decomposition, water balance, and peat  
388 accumulation. *Earth System Dynamics* 1, 1–21.
- 389 22. Page, S.E., and Baird, A.J. 2016. Peatlands and global change: response and resilience. *Annual Review of*  
390 *Environment and Resources* 41, 35–57.
- 391 23. Dubayah R, et al. (2014) The Global Ecosystem Dynamics Investigation. American Geophysical Union, Fall  
392 Meeting 2014 (AGU, San Francisco)
- 393 24. Page, S. E.; Rieley, J. O.; Shoty, O. W.; Weiss, D. Interdependence of peat and vegetation in a tropical peat  
394 swamp forest. *Phil. Trans. R. Soc. Lond. B* 354, 1885–1897 (1999).
- 395 25. Anderson, J.A.R. (1964) The structure and development of peat swamps of Sarawak and Brunei. *J. Trop.*  
396 *Geogr* 18, 7–16.
- 397 26. Andriess, J.P. (1972) *The Soils of West Sarawak (East Malaysia)*. Memoir 1, Vol. 1, Department of Agriculture,  
398 Sarawak, Malaysia.
- 399 27. Swindles, G. T.; Reczuga, M.; Lamentowicz, M.; Raby, C.L.; Turner, T.E.; Charman, D.J.; Gallego-Sala, A.  
400 "Ecology of testate amoebae in an Amazonian peatland and development of a transfer function for  
401 palaeohydrological reconstruction." *Microbial ecology* 68, no. 2 (2014): 284-298.
- 402